ADVANCED FUNCTIONAL MATERIALS
www.afm-journal.de

Materials Views
www.MaterialsViews.com

Impact of Bi Deficiencies on Ferroelectric Resistive Switching Characteristics Observed at p-Type Schottky-Like Pt/$Bi_{1-\delta}FeO_3$ Interfaces

Atsushi Tsurumaki, Hiroyuki Yamada, and Akihito Sawa**

This work reports a resistive switching effect observed at rectifying Pt/$Bi_{1-\delta}FeO_3$ interfaces and the impact of Bi deficiencies on its characteristics. Since Bi deficiencies provide hole carriers in $BiFeO_3$, Bi-deficient $Bi_{1-\delta}FeO_3$ films act as a p-type semiconductor. As the Bi deficiency increased, a leakage current at Pt/$Bi_{1-\delta}FeO_3$ interfaces tended to increase, and finally, rectifying and hysteretic current–voltage (*I–V*) characteristics were observed. In *I–V* characteristics measured at a voltage-sweep frequency of 1 kHz, positive and negative current peaks originating from ferroelectric displacement current were observed under forward and reverse bias prior to set and reset switching processes, respectively, suggesting that polarization reversal is involved in the resistive switching effect. The resistive switching measurements in a pulse-voltage mode revealed that the switching speed and switching ratio can be improved by controlling the Bi deficiency. The resistive switching devices showed endurance of $>10^5$ cycles and data retention of $>10^5$ s at room temperature. Moreover, unlike conventional resistive switching devices made of metal oxides, no forming process is needed to obtain a stable resistive switching effect in the ferroelectric resistive switching devices. These results demonstrate promising prospects for application of the ferroelectric resistive switching effect at Pt/$Bi_{1-\delta}FeO_3$ interfaces to nonvolatile memory.

1. Introduction

Continued advances in information technology rely on high-speed, large-capacity and low-power-consumption nonvolatile memories. However, as contemporary memory technologies such as flash memory are approaching their technological and physical miniaturization limits, it will be difficult to continue to improve the performance. As an alternative to contemporary flash memory, resistance random access memory (ReRAM)[1–3] based on resistive switching phenomena in metal oxides has attracted considerable attention because of its advantages in high-speed switching and high-density memory applications. The resistive switching phenomena have been observed in capacitor-like structures consisting of various metal oxides, such as multielemental perovskite-type oxides[4–7] and binary oxides,[8–12] and the observed resistive switching behaviors differ depending on the material. The variety of resistive switching behaviors observed suggests that there are some different mechanisms involved in the phenomena, and some possible mechanisms have been proposed so far. In terms of microscopic physics, the proposed mechanisms can be classified into two broad types:[1–3] thermochemical mechanisms and valence-change mechanisms. In the thermochemical mechanisms, a conductive filament is formed in an insulating matrix by an electroforming process, and the local redox reaction in a filament due to Joule heating induces resistive switching. In the valence-change mechanisms, electromigration of oxygen vacancies induces a change in the valence states of cations in a metal oxide, resulting in a change in the electronic states, with resultant alteration of the conductivity. ReRAMs based on both mechanisms have been intensively studied in recent years. However, since both mechanisms inevitably induce a chemical alteration of the metal oxides, there is concern for the reliability, such as the data retention and endurance. As a solution to the issue of reliability, resistive switching based on an electronic mechanism is being considered.

Ferroelectric resistive switching effects based on polarization reversal are particularly attractive, since polarization reversal does not induce a chemical alteration and is an intrinsically fast phenomenon. The resistive switching effect in a ferroelectric niobium oxide was first reported in the 1970s,[13] and since then, ferroelectric perovskite titanates[14–20] have become the focus of attention in the study of ferroelectric resistive switching. Ferroelectric resistive switching effects can be categorized into two types depending on the mechanism involved. The tunnel electroresistance effect[17–19,21] relies on a change in tunneling barrier height induced by polarization reversal. For the resistive switching of a ferroelectric Schottky diode,[14–16,20,22] a Schottky-like barrier forms at the interface between a metal electrode and conductive ferroelectric oxide, and the potential profile of the Schottky-like barrier is reversibly modified by the polarization flipping. Ferroelectric resistive switching effects have usually

Dr. A. Tsurumaki, Dr. H. Yamada, Dr. A. Sawa
National Institute of Advanced Industrial Science and Technology (AIST)
Tsukuba, Ibaraki 305-8562 Japan
E-mail: a.sawa@aist.go.jp; a-tsurumaki@aist.go.jp

DOI: 10.1002/adfm.201102883

been studied in terms of hysteretic current–voltage (*I–V*) characteristics,[14–17,19,20,22] but investigation of the switching characteristics in the pulse-voltage mode is needed for memory applications. Recently, the switching operation in the pulse-voltage mode has been reported in switchable diode devices consisting of a multiferroic oxide $BiFeO_3$ (BFO):[23] Repeatable resistive switching has been achieved by applying pulsed voltage stresses with $V = \pm 10$ V and duration (τ_P) of 1 μs. In the switchable diode devices,[23–25] an n-type BFO, in which electron carriers are provided by oxygen vacancies, is usually employed, and Schottky-like barriers form at both the top and bottom metal/BFO interfaces. The polarization reversal modulates the potential profile of the Schottky-like barriers and switches the rectification direction. The switchable diode effect is characterized as bipolar-type switching with *noncrossing* hysteretic *I–V* characteristics, which are basically *symmetric* with respect to the applied voltage polarity. On the other hand, the resistive switching of ferroelectric Schottky diodes[14–16,20,22] shows bipolar-type switching with *zero-crossing* hysteretic *I–V* characteristics, which are *asymmetric* with respect to the applied voltage polarity. From a technological viewpoint, a device having asymmetric and nonlinear *I–V* characteristics seems to be suitable for large-capacity memory applications, because it allows fabrication of a cross-point memory array without any selection element, such as a diode.[26]

In this paper, we report the resistive switching effect observed at a rectifying Pt/$Bi_{1-\delta}FeO_3$ interface. Unlike previous studies on switchable diodes,[23–25] we used a p-type semiconductive $Bi_{1-\delta}FeO_3$ film as a switching element, since its conductivity, as well as the depletion layer width of a Schottky-like barrier, can be controlled by changing the Bi deficiency concentration, δ. Also, studying the Bi-deficiency dependence of the resistive switching characteristics can provide clues to the mechanism involved and should reveal how to control the device characteristics. Pt/$Bi_{1-\delta}FeO_3$ interfaces with a large δ showed bipolar-type switching with zero-crossing hysteretic *I–V* characteristics without rectification-direction flipping. The experimental results suggest that the nonepitaxial nature of the Pt/$Bi_{1-\delta}FeO_3$ interface plays a crucial role in the emergence of the resistive switching effect. *I–V* measurements with a higher voltage-sweep frequency (*f*) revealed that ferroelectric displacement charges flowed prior to set and reset switching processes, suggesting that polarization reversal induces the resistive switching effect. From a technological viewpoint, resistive switching characteristics and reliability in pulse-voltage mode were also evaluated.

2. Results and Discussions

2.1. Hysteretic *I–V* Characteristics

We fabricated Au/Pt/BFO/$SrRuO_3$(SRO) layered structures on $SrTiO_3$ (001) single-crystal substrates. A 50 nm-thick SRO bottom electrode was grown on the substrates prior to a 100 nm-thick BFO layer by using pulsed laser deposition (PLD). Both BFO and SRO layers were confirmed to be epitaxially grown on the $SrTiO_3$ substrates from X-ray diffraction measurements. An Au(100 nm)/Pt(10 nm) top electrode was deposited on the BFO layer through a shadow mask (pad size of 100 μm × 100 μm) by using electron-beam evaporation.

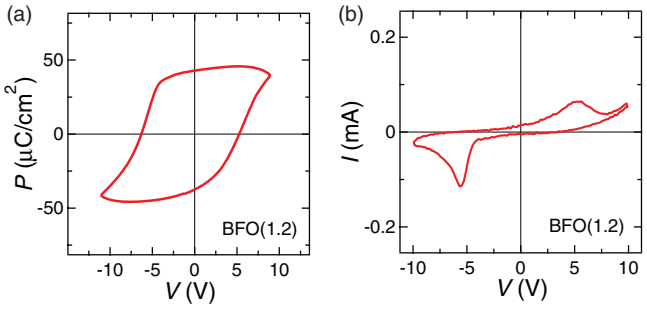

Figure 1. a) *P–V* and b) *I–V* characteristics of an Au/Pt/BFO(1.2)/SRO device, measured at $f = 1$ kHz.

In PLD, the chemical composition in the source target is generally transferred to the grown film. However, since Bi is a volatile element, the Bi content in the PLD-grown BFO film is usually smaller than that in the source target.[27,28] In order to control the Bi content in the BFO films, therefore, we deposited the films from source targets with several Bi/Fe ratios (*r*) of 1.2, 1.1, and 1.0, and the Bi/Fe ratios in the BFO films (r_f) were estimated from inductively coupled plasma atomic emission spectrometry. For the typical deposition conditions used in the present study, the films deposited from the targets with *r* of 1.2 were confirmed to be practically stoichiometric with $r_f = 0.95$ (±0.01). On the other hand, the films deposited from the targets with *r* of 1.1 and 1.0 had small r_f of 0.83 (±0.01) and 0.76 (±0.05), respectively. This result suggests that those films had large Bi deficiency δ. Hereafter, the films deposited from the targets with *r* of 1.2, 1.1, and 1.0 are denoted as BFO(1.2), BFO(1.1), and BFO(1.0), respectively.

Figure 1 exhibits the polarization–voltage (*P–V*) and *I–V* characteristics of the Au/Pt/BFO(1.2)/SRO device measured at $f = 1$ kHz. The *I–V* curve is slightly asymmetric, which is thought to be due to the formation of a Schottky-like barrier at the Pt/BFO interface, as will be discussed later. Because of the small Bi deficiency, the leakage current in the device was small enough to measure the polarization, and a spontaneous polarization (P_r) of ~40 μC cm^{-2} was obtained. This value is slightly smaller than typical values reported for [001]-oriented BFO films (~60 μC cm^{-2}).[29,30] This may result from leakage charges caused by Bi deficiencies and from the existence of pinned (not switchable) domains due to epitaxial strain from the substrate. As δ was increased, the leakage current tended to increase. The BFO(1.1) and BFO(1.0) devices no longer exhibited the ideal ferroelectric *P–V* loop, but showed zero-crossing hysteretic *I–V* characteristics, as shown in **Figure 2**a. In addition to hysteretic behavior, clear rectifying characteristics were observed, suggesting the formation of a Schottky-like barrier. Note that the positive direction of the bias voltage was defined as the direction causing current to flow from the SRO bottom electrode layer to the Pt top electrode. These characteristics suggest that only one interface serves as the active source of the rectification and the hysteretic behavior. In order to confirm which interface is the active source, we prepared an Au/SRO/BFO(1.1)/SRO device and measured the *I–V* characteristics. As seen in Figure 2c, the Au/SRO/BFO(1.1)/SRO device showed ohmic *I–V* characteristics without hysteresis. This provides evidence that the Pt/$Bi_{1-\delta}FeO_3$ interfaces with a larger δ exhibit hysteretic and

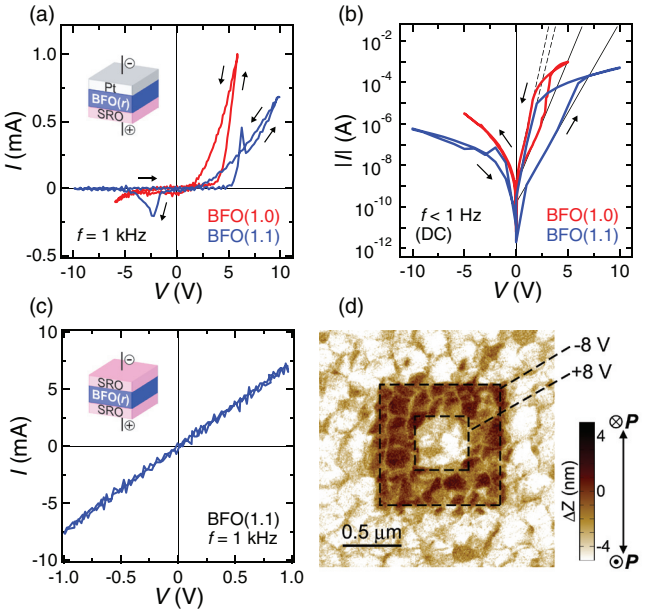

Figure 2. a) *I* – *V* characteristics of Au/Pt/BFO(1.1)/SRO and Au/Pt/BFO(1.0)/SRO devices. Triangular-wave voltages of $f = 1$ kHz were swept as 0 V → +10 V → –10 V → 0 V for the BFO(1.1) device and 0 V → +6 V → –6 V → 0 V for the BFO(1.0) device. b) *I* – *V* characteristics of Au/Pt/BFO(1.1)/SRO and Au/Pt/BFO(1.0)/SRO devices measured in DC mode ($f < 1$ Hz). DC voltages were swept as 0 V → +10 V → –10 V → 0 V for the BFO(1.1) device and 0 V → +5 V → –5 V → 0 V for the BFO(1.0) device. Solid and broken straight lines in b) are fits to the Schottky model for HRS and LRS, respectively. c) *I* – *V* characteristic of an Au/SRO/BFO(1.1)/SRO device, measured at $f = 1$ kHz. d) Out-of-plane piezoresponse force microscope image of a BFO(1.0)/SRO sample. The image was obtained with a bias voltage of +3 V at 5 kHz after poling processes (see text). Voltage was applied from a biased stage to a grounded tip, and the dark contrast in the image corresponds to downward polarization.

rectifying *I*–*V* characteristics. Moreover, based on the rectification direction, we can consider that a p-type Schottky-like barrier forms at the Pt/$Bi_{1-\delta}FeO_3$ interfaces.

Figure 2b shows the DC *I*–*V* characteristics (measured at $f <$ 1 Hz) plotted on a semilogarithmic scale for the Au/Pt/BFO(*r*)/SRO devices with $r = 1.1$ and 1.0. Here, we define a high resistance state (HRS) and a low resistance state (LRS) for lower and upper branches of the hysteretic *I*–*V* curve, respectively. For forward bias (positive bias), the log *I*–*V* curves in the HRS of both devices are nearly a straight line in the lower voltage region. This result seems to agree with the Schottky barrier model, meaning that the thermionic emission process is predominant in the HRS. However, the ideality factors extracted from the *I*–*V* curves by using the thermionic emission model were 20 and 14 for the devices with $r = 1.1$ and 1.0, respectively, and were much larger than the ideal value of 1 in a semiconductor Schottky junction (see Supporting Information). Such a large ideality factor has been reported in the switchable BFO diode[24] and the metal/porous-Si/Si diode.[31] In the metal/porous-Si/Si diode, the rectifying behavior originates from the band bending inside the Si layer at its interface to the porous-Si layer and the porous-Si layer acts as a barrier to the carrier conduction. The large series resistance originated from the porous-Si layer results in the large ideality factor of the metal/porous-Si/Si diode. From the large *n* values in our devices, thus, we can expect that an additional barrier layer may form between Pt-electrode and BFO layer, as will be discussed later. For the LRS, the rectifying behavior was observed and the log *I*–*V* curves in forward bias fit with the broken straight lines, suggesting that the thermionic emission process is predominant in the LRS. However, the extracted ideality factors in the LRS were also much larger than 1. If the thermionic emission process predominates the carrier conduction in both the HRS and LRS for the devices, the larger currents in the LRS are attributable to a reduced barrier height and/or width with respect to the HRS.

Note that the resistance values in the HRS and LRS varied from device to device and from chip to chip. One possibility could be the properties variation of the interfacial layer. Developing the means for control of the interfacial-layer properties such as thickness and band gap can improve the characteristic variation in the devices.

In order to confirm the existence of ferroelectricity in Bi-deficient, conductive BFO layers, the BFO(1.0) film, which was the most conductive BFO film in the present study, was characterized with a piezoresponse force microscope (PFM). Figure 2d shows the piezoresponse characteristics of the BFO(1.0)/SRO sample. A 1 μm × 1 μm area was poled downward with a voltage of –8 V, inside which a 0.5 μm × 0.5 μm area was poled upward with a voltage of +8 V. Depending on the poling direction, a positive or negative piezoresponse was observed. This result is quite similar to that of an oxygen-deficient n-type BFO film.[23] This suggests that ferroelectricity can exist in conductive BFO films regardless of the carrier type and the defect type.

Here, we discuss details of the hysteretic *I*–*V* characteristics. **Figure 3**a shows the *I*–*V* curve of an Au/Pt/BFO(1.1)/SRO device, which is the same *I*–*V* curve as in Figure 2a. In this measurement, the voltage was swept as 0 V → +10 V → –10 V → 0 V at $f = 1$ kHz. Positive and negative current peaks were observed at $V = +6.3$ V and –2.3 V, respectively. The resistance state of the device changed from the HRS to the LRS after the positive current peak, whereas it changed from the LRS to the HRS after the negative current peak. This switching behavior suggests that the resistive switching is mediated by a large current flow in the device. To elucidate the origin of the current peaks, we measured the *I*–*V* characteristics at a reduced *f* of 100 Hz and observed no current peak, as shown in Figure 3b. This result suggests that the origin of the current peaks is a transient current, such as ferroelectric displacement current. In order to identify a ferroelectric displacement current as the origin of the current peaks, we estimated the polarization value as a function of *V* for a negative bias voltage (reverse bias) from a time integration of *I*(*t*) (see Supporting Information). The inset of Figure 3a exhibits the *P*–*V* curve obtained from the *I*–*V* curve in Figure 3a. The P_r value was estimated to be ~40 μC cm^{-2}, which roughly coincides with that obtained from the Au/Pt/BFO(1.2)/SRO device (Figure 1a). This result suggests that the ferroelectric displacement current is the predominant cause of the observed current peaks, and that polarization reversal is involved in the resistive switching in the device.

In the repeatedly measured *I*–*V* characteristics, we found a useful property of our devices, i.e., a forming-free resistive switching behavior. For conventional ReRAMs based on

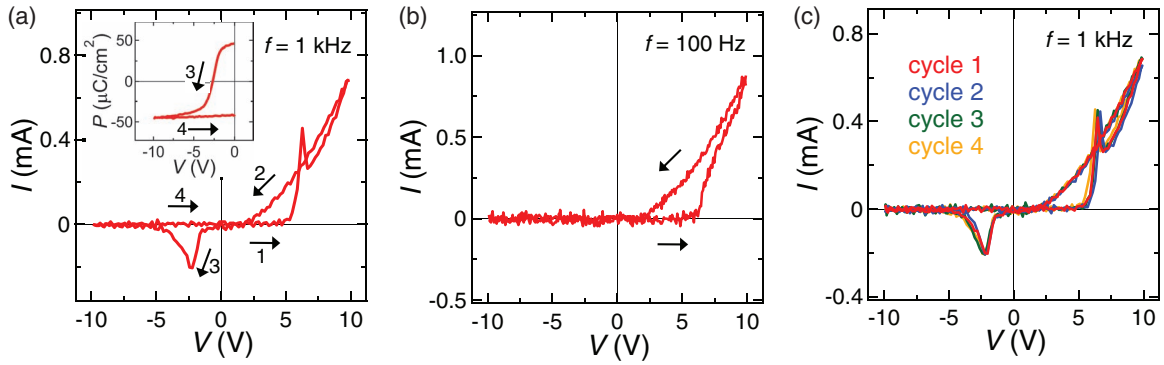

Figure 3. *I–V* characteristics of an Au/Pt/BFO(1.1)/SRO device measured at frequencies, *f*, of a) 1 kHz and b) 100 Hz. Arrows and numbers in the figures indicate the sequence of the hysteretic current loop. The inset in a) shows *P – V* characteristic of the device obtained from a time integration of *I* (*t*) (see Supporting Information). c) Repetition behavior of the hysteretic *I–V* characteristics of the Au/Pt/BFO(1.1)/SRO device.

a thermochemical mechanism, a so-called forming process is usually necessary to obtain stable resistive switching.[1–3] The forming process is believed to generate conductive filaments in an insulating metal oxide.[32] Since a large voltage and current are needed to induce the forming process in a memory cell, a forming-free memory cell would be desirable in meeting the requirements of commercial products. Figure 3c displays repeatedly measured *I–V* characteristics of the Au/Pt/BFO(1.1)/SRO device. The initial *I–V* curve (1st cycle) was almost identical to those obtained from the second, third, and fourth measurements. This result suggests that no forming process is needed to obtain stable resistive switching in our device. This lack of need for a forming process suggests that the observed resistive switching does not rely on the formation of conductive filaments.

For the filament-type resistive switching, a forming voltage increases with increasing the oxide layer thickness, whereas set and reset switching voltages are independent of the oxide layer thickness. The thickness dependence of the resistive switching characteristics can thus give a clue to understanding the mechanism of the resistive switching. **Figure 4** shows the thickness dependence of the *I–V* characteristics of the BFO(1.0) devices. Set and reset switching voltages decreased as the thickness of BFO(1.0) layer was decreased. It should be noted that the BFO(1.0) devices shown in Figure 4 also did not need a forming process to obtain stable resistive switching. Moreover, for the filament-type resistive switching, the current suddenly increases at the forming voltage and the current compliance is essential for preventing the hard breakdown. However, our devices did not need the current compliance for the resistive switching even in the initial stage, suggesting that no filament formation takes place in our devices.

Our devices show other characteristics different from the filament-type resistive switching device. The capacitance of our device changes depending on the resistance states (Supporting Information). For the interfacial resistive switching, the capacitances change depending on resistance states.[2] For the conductive-filament resistive switching, on the other hand, it has been reported that the capacitances in HRS and LRS are almost identical.[33] Therefore, the capacitive switching of our devices suggests that the filament-type mechanism does not seems to be involved in the resistive switching observed in our devices.

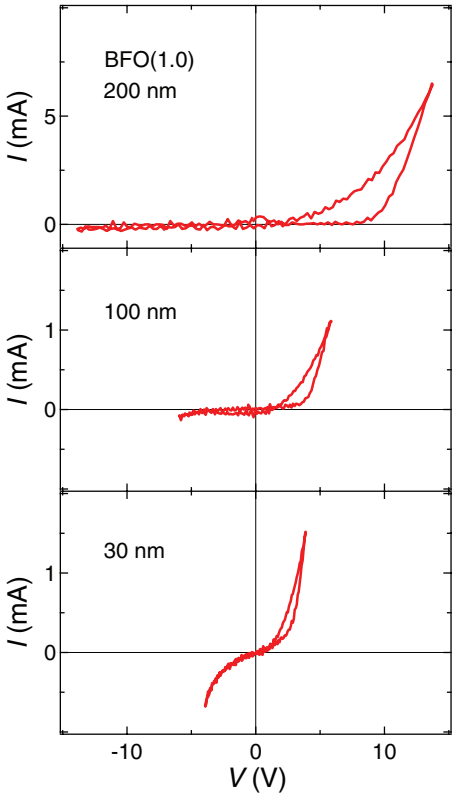

Figure 4. *I–V* characteristic of Au/Pt/BFO(1.0)/SRO devices with BFO layer thicknesses of 200 nm, 100 nm, and 30 nm, measured at *f* = 1 kHz.

2.2. Modulation of Schottky-Like Barrier

The *I–V* measurements of the Au/Pt/BFO(*r*)/SRO and Au/SRO/BFO(*r*)/SRO devices revealed that the resistive switching effect emerges at a rectifying Pt/BFO(*r*) interface. The rectification direction indicates that a p-type Schottky-like barrier forms at the Pt/BFO(*r*) interface. The PFM measurement confirmed the existence of ferroelectric polarization in a conductive BFO film, and the current peaks observed in the *I–V* characteristics

of the Au/Pt/BFO(1.1)/SRO device suggest that polarization reversal is involved in the resistive switching effect. From these experimental results, we can attribute the observed resistive switching phenomenon to a change in the potential profile of a Schottky-like barrier formed at the Pt/BFO(r) interface due to the polarization reversal.

In the present study, we intentionally introduced Bi deficiency in the BFO films. The Bi deficiency δ increases the valence of Fe ions and confers p-type characteristics to $Bi_{1-\delta}FeO_3$ films. For contact between a metal and p-type semiconductor, the Schottky barrier height should be the energy difference between the metal work function and the top of the valence band of a p-type semiconductor. Since the work functions of SRO and Pt are ~5.2 eV and ~5.3 eV, respectively, and the electron affinity and the band gap of BFO are ~3.3 eV and ~2.8 eV, respectively,[34] the p-type Schottky barrier heights at SRO/BFO(r) and Pt/BFO(r) interfaces can be estimated to be less than 0.9 eV (Figure S2 in Supporting Information). We should note that, in spite of the similar Schottky barrier heights for both interfaces, ohmic and Schottky-like contacts were realized at the SRO/BFO(r) and Pt/BFO(r) interfaces, respectively. This difference cannot be understood from a conventional Schottky model. Thus, we consider differences in electrode materials and crystallinity between them as a possible origin of the different interfacial transport properties.

In ferroelectric capacitors, it is well known that a thin dielectric layer often forms between a metal electrode and a ferroelectric oxide layer.[35–38] This interfacial layer is called a passive layer or dead layer. The formation of such an interfacial layer has been reported recently in the BFO capacitors.[38] Although structural and physical properties of the interfacial layer are still under debate, the interfacial disorder and/or defects may suppress ferroelectricity at the interface. Moreover, the properties of the interfacial layer depend on electrode materials and crystallinity at the interface.[35–37] When nonepitaxial novel-metal films such as Au or Pt are used as electrodes, the residual polarization of the $Pb(Zr,Ti)O_3$ (PZT) film decreases rapidly with switching cycle number and the coercive field of the PZT film is much larger than that of bulk ceramics.[36,37] On the other hand, the use of epitaxial oxide films as electrodes for the PZT-film capacitors can improve fatigue properties and the coercive field due to the suppression of the interfacial-layer formation.[36,37]

In our devices, the SRO/BFO(r) interface is an epitaxial contact, whereas the Pt/BFO(r) interface is a nonepitaxial contact. At the nonepitaxial Pt/BFO(r) interface, thus, an interfacial layer may form and act as a barrier layer for the hole-carrier conduction, as illustrated in **Figure 5**. The fact that the large ideality factors were extracted from the I–V characteristics supports the formation of an interfacial layer, as discussed previously. Moreover, the interfacial disorder and/or defects at the nonepitaxial Pt/BFO(r) interface may reduce an effective acceptor concentration at the interface. At the epitaxial SRO/BFO(r) interface, on the other hand, an interfacial layer may form but its thickness can be expected to be much thinner as compared to that at the nonepitaxial Pt/BFO(r) interface. Because of the thin interfacial layer, the contact resistance at the epitaxial SRO/BFO(r) interface is much lower than that at the nonepitaxial Pt/BFO(r) interface, and the epitaxial SRO/BFO(r) interface shows practically ohmic characteristics (Figure 2c). Therefore, our device

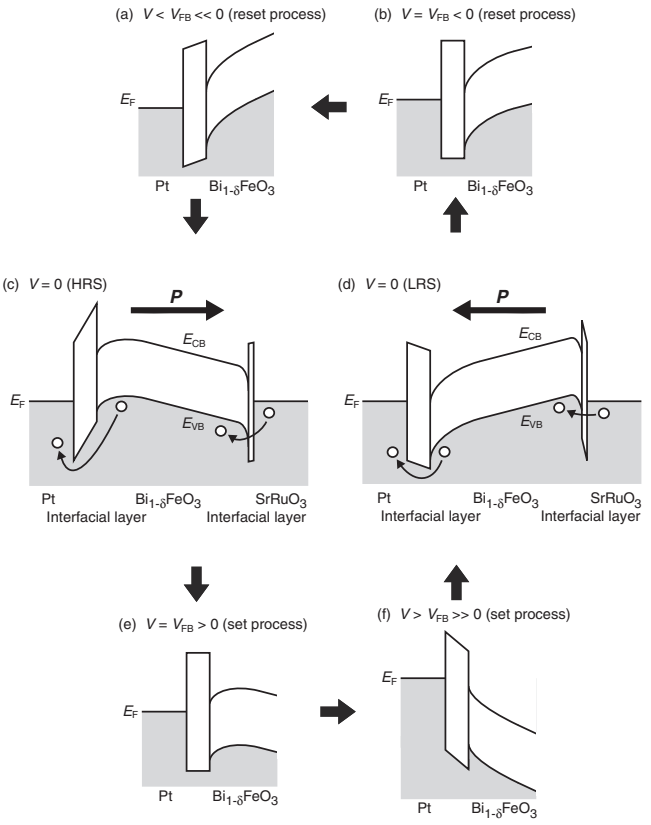

Figure 5. Schematic energy-band diagrams of a Pt/BFO(r)/SRO device with interfacial layers c) in the HRS at $V = 0$ and d) in the LRS at $V = 0$. The details of the estimation of the band diagrams are described in supporting information. In the HRS, a downward polarization increases the band bending of the interfacial layer and the depletion layer and thus the effective barrier height to hole carrier conduction increases. In the LRS, an upward polarization decreases the effective barrier height. Schematic energy-band diagram of the Pt/BFO(r) interface b) for $V = V_{FB} < 0$ and a) for $V < V_{FB} << 0$ in the reset process. Schematic energy-band diagrams of the Pt/BFO(r) interface e) for $V = V_{FB} > 0$ and f) for $V > V_{FB} >> 0$ in the set process.

structure can be viewed as a metal/insulator/p-type ferroelectric semiconductor/insulator/metal structure. Recently, Mayer et al., have discussed the resistive switching characteristics observed in the ferroelectric capacitors based on the band diagram of a metal/insulator/ferroelectric oxide/insulator/metal structure.[16] Here, taking into account the formation of Schottky-like barrier, we modify the model proposed by Mayer et al.[16] in order to explain the resistive switching characteristics observed in our device. The details of our model (possible band diagrams of our device) are described in supporting information (Figure S3, Supporting Information). Owing to the interfacial layer, the potential profile at the Pt/interfacial layer/BFO (Pt/IL/BFO) interface changes significantly depending on the polarization direction. For the downward polarization state (Pt → SRO), large band bending appears in the interfacial layer as well as in the depletion layer at the Pt/IL/BFO interface. For the upward polarization state (SRO → Pt), on the other hand, the insulator bands are bent oppositely at the Pt/IL/BFO interface, since the opposite polarization charge appears at the interface. In this

model, the interfacial layer and the depletion layer act as an effective barrier to the hole-carrier conduction at the Pt/IL/BFO interface. As seen in Figure 5, the effective barrier height in the downward polarization state is higher than that in the upward polarization state. The variable barrier height depending on the polarization directions controls hole-carrier conduction at the Pt/BFO(r) interface, which is a possible mechanism of the resistive switching effect.

Based on the band diagrams, the asymmetry of the switching voltages between the set and reset processes observed in Figure 2a can be explained. In order to switch the resistance state from the HRS to LRS (set process), the polarization is flipped from the downward state to the upward state. To obtain the upward polarization state, the BFO bands are bent downward by applying positive voltages to the SRO electrode. However, since the interfacial layer bands and the BFO bands in the depletion layer at the Pt/BFO interface are bent upward in the HRS, those bands should be bent in the opposite direction (downward) by applying positive voltages prior to the polarization flip. In the LRS, the interfacial layer bands are bent downward whereas the BFO bands in the depletion layer are bent upward at the Pt/BFO interface. For the switching from the LRS to HRS (reset process), therefore, only the interfacial layer bands should be bent in the opposite direction (upward) by applying negative voltages prior to the polarization flip. Here, we defined the voltage which is needed to realize a flat-band like state in the interfacial layer as V_{FB} and the potential gradient of the interfacial layer bands as φ_{IL}. In the proposed model (Figure 5 and Figure S3c, Supporting Information), since $|\varphi_{IL}|$ in the HRS is larger than that in the LRS, $|V_{FB}|$ in the set process is larger than that in the reset process. Moreover, in the set process, the BFO bands in the depletion layer should be bent downward prior to the polarization flip (Figure 5f). As a result, the set-switching voltage $|V_{set}|$ is larger than the reset-switching voltage $|V_{reset}|$.

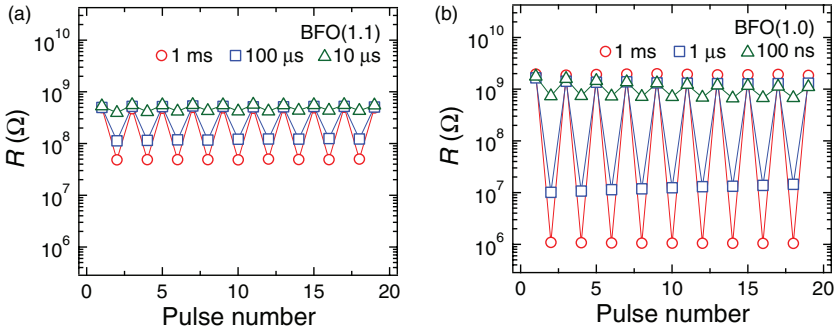

Figure 6. Resistive switching behaviors of a) an Au/Pt/BFO(1.1)/SRO device and b) an Au/Pt/BFO(1.0)/SRO device, measured in pulse-voltage mode with various τ_p. Pulsed voltage stresses of $V_p = \pm 8$ V or ± 7 V were respectively applied to the devices. Resistance values were evaluated from current values at $V = +1$ V.

2.3. Switching Characteristics in Pulse-Voltage Mode

We investigated the pulsed-voltage-induced resistive switching characteristics of our devices. **Figure 6** shows the pulse-duration time (τ_p) dependence of the resistive switching characteristics of Au/Pt/BFO(1.1)/SRO and Au/Pt/BFO(1.0)/SRO devices. We found that the R_H values were nearly independent of τ_p, whereas the R_L values increased with decreasing τ_p, where R_H and R_L are the resistances in the HRS and LRS, respectively. This result suggests that it is difficult to induce switching from the HRS to the LRS as compared with switching from the LRS to the HRS, and the switching characteristics, such as switching ratio (R_H/R_L), are governed by the switching process from the HRS to the LRS. These characteristics are attributable to the asymmetric switching of our device: The set-switching voltage $|V_{set}|$ is larger than the reset-switching voltage $|V_{reset}|$, as seen in Figure 2a. As seen in Figure 6a, R_H/R_L of the Au/Pt/BFO(1.1)/SRO device decreased with decreasing τ_p, and almost no switching was observed at $\tau_p = 1$ µs (data not shown). For the Au/Pt/BFO(1.0)/SRO device, on the other hand, clear resistive switching behavior with $R_H/R_L \approx 2$ was observed, even at $\tau_p = 100$ ns, as shown in Figure 6b. This enhancement of the switching speed led to an increase in R_H/R_L. For the same $\tau_p =$ 1 ms, R_H/R_L of the Au/Pt/BFO(1.0)/SRO device was more than 10^3, whereas that of the Au/Pt/BFO(1.1)/SRO device was only about 10. These results suggest that the switching speed and ratio can be enhanced by increasing the Bi deficiency. Although the detailed mechanism of the Bi-deficiency dependence of the switching characteristics is still unclear, the decrease in the switching voltages by increasing the Bi deficiency may play a crucial role for the enhancement of the switching speed and ratio.

Next, in order to evaluate the potential of our resistive-switching devices for nonvolatile memory applications, we performed data retention and endurance tests. **Figure 7**a exhibits the results of data retention of the Au/Pt/BFO(1.0)/SRO device obtained at room temperature and 125 °C. After applying 10^3 cycles of voltage stresses with an amplitude of

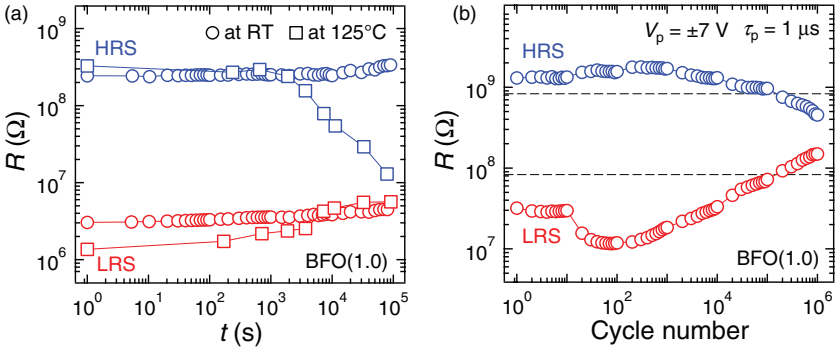

Figure 7. a) Data retention and b) endurance characteristics of an Au/Pt/BFO(1.0)/SRO device. Broken lines in b) represent a memory window of $R_H/R_L = 10$.

$V_p = \pm 7$ V and $\tau_p = 10$ μs at room temperature, the resistance state of the device was set to the LRS or HRS by applying a voltage pulse with $\tau_p = 10$ μs and $V_p = +7$ or -7 V, respectively, and then the data retention characteristics were measured. At room temperature, both R_H and R_L slightly increased with time, but the device kept the R_H/R_L ratio of ~10^2 for 10^5 s. This nonvolatility of our device is attributable to the intrinsic nonvolatile nature of ferroelectric polarization. At 125 °C, however, R_H decreased rapidly with time at $t > 10^3$ s. Based on our proposed model (Figure 5), the decrease in R_H suggests that the polarization reversal from the downward direction (Pt → SRO) to the upward direction (SRO → Pt) takes place as the temperature is increased.

For the endurance test, we applied cycles of voltage pulses with $V_p = \pm 7$ V and $\tau_p = 1$ μs to the Au/Pt/BFO(1.0)/SRO device. R_H and R_L values were evaluated from current values at $V = +1$ V. As shown in Figure 7b, R_H (R_L) initially increased (decreased) with cycle number and then monotonically decreased (increased) after ~10^3 (~10^2) cycles. As a result, R_H/R_L initially increased up to around 10^2 cycles and then started to decrease. This switching-cycle dependence of the R_H/R_L is similar to those of P_r and J_{diode}, the latter being defined as the difference between on and off current densities, observed in switchable diodes.[23] The initial increase in P_r and J_{diode} is attributed to depinning of preferred domains.[30] After the depinning process, polarization fatigue becomes clear, and thus P_r and J_{diode} decreases with cycle number. Because of the similar dependence on switching cycles, the depinning process and the polarization fatigue seem to be involved in the endurance mechanism of our devices. Our device showed a large R_H/R_L ratio of >10 up to 10^5 cycles, and the R_H/R_L ratio was as large as 3 even at 10^6 cycles. This endurance is better than that of switchable diodes.[23,24] However, for achieving practical use of ferroelectric resistive memory, the retention at higher temperature as well as the endurance should be improved. Further investigations on the degradation and fatigue mechanisms will provide clues to improving the device characteristics.

3. Conclusions

We have studied the resistive switching characteristics at p-type Schottky-like Pt/$Bi_{1-\delta}FeO_3$ interfaces in terms of *I–V* measurements at a high voltage-sweep frequency *f* and pulsed-voltage switching measurements. The Au/Pt/$Bi_{1-\delta}FeO_3$/$SrRuO_3$ devices that we fabricated showed bipolar resistive switching with a zero-crossing hysteretic *I–V* characteristic. In the *I–V* characteristics measured at $f = 1$ kHz, positive and negative current peaks originating from ferroelectric displacement charges were observed prior to set and reset switching processes, respectively. Piezoresponse force microscope (PFM) measurements revealed the coexistence of ferroelectricity and conductivity in the semiconductive $Bi_{1-\delta}FeO_3$ films. Based on the experimental results, we propose that the modification of the potential profile of the barrier at the Pt/$Bi_{1-\delta}FeO_3$ interface induced by polarization reversal is responsible for the resistive switching phenomenon. The current study has also demonstrated that the device performance, such as switching speed and ratio, can be improved by controlling the Bi deficiency. Moreover, the devices showed promising characteristics for use as nonvolatile memories, including stable resistive switching without the need for any forming process, data retention of >10^5 s at room temperature, and endurance of >10^5 cycles.

4. Experimental Section

$Bi_{1-\delta}FeO_3$(100 nm)/$SrRuO_3$(50 nm) layered structures were deposited on $SrTiO_3$ (100) substrates by pulsed laser deposition (PLD) at a substrate temperature of 700–720 °C under an oxygen pressure of 25–30 mTorr. In order to obtain $Bi_{1-\delta}FeO_3$ layers with different Bi deficiencies δ, we prepared several ceramic targets having different Bi/Fe ratios of 1.2, 1.1, and 1.0. The Bi/Fe ratio r_f in the films was evaluated by inductively coupled plasma atomic emission spectrometry (ICP) at Hitachi Kyowa Engineering Co., Ltd.. Four-circle X-ray diffraction measurements (Philips X'Pert PRO MRD) were performed to evaluate the lattice parameters and the crystal structure.

For the Au/Pt/$Bi_{1-\delta}FeO_3$/$SrRuO_3$ devices, an Au(100 nm)/Pt(10 nm) layered electrode was deposited by electron beam evaporation through a shadow mask (100 μm × 100 μm). For the Au/$SrRuO_3$/$Bi_{1-\delta}FeO_3$/$SrRuO_3$ devices, a $SrRuO_3$(50 nm)/$Bi_{1-\delta}FeO_3$(100 nm)/$SrRuO_3$(50 nm) layered structure was deposited on a $SrTiO_3$ substrate by PLD, and then an Au(100 nm) layer was deposited by electron beam evaporation. An Au/$SrRuO_3$/$Bi_{1-\delta}FeO_3$/$SrRuO_3$ layered structure was patterned into a device with dimensions of 100 μm × 100 μm using photolithography and argon ion milling.

I–V and *P–V* characteristics of the devices were measured with a ferroelectric testing system (Toyo Corp. FCE-1) consisting of a current/charge-voltage converter (Toyo Corp. Model 6252), an arbitrary waveform generator (Biomation 2414B), and an analogue-to-digital converter (WaveBook 516). DC *I–V* characteristics of the devices were also measured by using a source measure unit (Keithley 238). For pulsed-voltage measurements, voltage pulses were applied to a device by using an arbitrary waveform generator (Agilent 33250A) and were monitored by using an oscilloscope (Agilent DSO80604B), and resistance values, i.e. current values at $V = +1$ V, were measured by using Keithley 238. The read current sensitivity of Keithley 238 is 0.01 pA. Capacitance–voltage characteristics were measured by using an impedance analyzer (Agilent 4294A). In all measurements of electronic properties, top electrodes were grounded and voltages were applied from bottom electrodes. Piezoresponse measurements of $BiFeO_3$ layers were performed by using a scanning probe microscope with a CoCr-coated Si cantilever tip (SII NanoTechnology E-sweep scanning probe microscope) at the Foundation for Promotion of Material Science and Technology of Japan.

Supporting Information

Supporting Information is available from the Wiley Online Library or from the author.

Acknowledgements

The authors would like to thank Prof. Tokura and Prof. Kawasaki for useful discussions. This work was supported in part by the Japan Society for the Promotion of Science (JSPS) through the "Funding Program for World-Leading Innovative R&D on Science and Technology (FIRST Program)," initiated by the Council for Science and Technology Policy (CSTP), and a Grant-in-Aid for Scientific Research (No. 22360280).

Received: November 28, 2011
Published online: January 18, 2012

[1] R. Waser, M. Aono, *Nat. Mater.* **2007**, *6*, 833.
[2] A. Sawa, *Mater. Today* **2008**, *11*, 28.
[3] R. Waser, R. Dittmann, G. Staikov, K. Szot, *Adv. Mater.* **2009**, *21*, 2632.
[4] S. Q. Liu, N. J. Wu, A. Ignatiev, *Appl. Phys. Lett.* **2000**, *76*, 2749.
[5] A. Beck, J. G. Bednorz, Ch. Gerber, C. Rossel, D. Widmer, *Appl. Phys. Lett.* **2000**, *77*, 139.
[6] Y. Watanabe, J. G. Bednorz, A. Bietsch, Ch. Gerber, D. Widmer, A. Beck, S. J. Wind, *Appl. Phys. Lett.* **2001**, *78*, 3738.
[7] A. Sawa, T. Fujii, M. Kawasaki, Y. Tokura, *Appl. Phys. Lett.* **2004**, *85*, 4073.
[8] T. W. Hickmott, *J. Appl. Phys.* **1962**, *33*, 2669.
[9] I. G. Baek, M. S. Lee, S. Seo, M. J. Lee, D. H. Seo, D.-S. Suh, J. C. Park, S. O. Park, H. S. Kim, I. K. Yoo, U.-I. Chung, J. T. Moon, *IEDM Tech. Dig.* **2004**, 587.
[10] B. J. Choi, D. S. Jeong, S. K. Kim, C. Rohde, S. Choi, J. H. Oh, H. J. Kim, C. S. Hwang, K. Szot, R. Waser, B. Reichenberg, S. Tiedke, *J. Appl. Phys.* **2005**, *98*, 033715.
[11] K. Kinoshita, T. Tamura, M. Aoki, Y. Sugiyama, H. Tanaka, *Appl. Phys. Lett.* **2006**, *89*, 103509.
[12] D. B. Strukov, G. S. Snider, D. R. Stewart, R. S. Williams, *Nature* **2008**, *453*, 80.
[13] L. Esaki, R. B. Laibowitz, P. J. Stiles, *IBM. Tech. Discl. Bull.* **1971**, *13*, 2161.
[14] P. W. M. Blom, R. M. Wolf, J. F. M. Cillessen, M. P. C. M. Krijin, *Phys. Rev. Lett.* **1994**, *73*, 2107.
[15] A. Schmehl, F. Lichtenberg, H. Bielefeldt, J. Mannhart, D. G. Schlom, *Appl. Phys. Lett.* **2003**, *82*, 3077.
[16] R. Meyer, J. R. Contreras, A. Petraru, H. Kohlstedt, *Int. Ferroelectrics* **2004**, *64*, 77.
[17] P. Maksymovych, S. Jesse, P. Yu, R. Ramesh, A. P. Baddorf, S. V. Kalinin, *Science* **2009**, *324*, 1421.
[18] V. Garcia, S. Fusil, K. Bouzehouane, S. Enouz-Vedrenne, N. D. Mathur, A. Barthélémy, M. Bibes, *Nature* **2009**, *460*, 81.
[19] A. Gruverman, D. Wu, H. Lu, Y. Wang, H. W. Jang, C. M. Folkman, M. Y. Zhuravlev, D. Felker, M. Rzchowski, C.-B. Eom, E. Y. Tsymbal, *Nano Lett.* **2009**, *9*, 3539.
[20] L. Pintilie, V. Stancu, L. Trupina, I. Pintilie, *Phys. Rev. B* **2010**, *82*, 085319.
[21] M. Y. Zhuravlev, R. F. Sabirianov, S. S. Jaswal, E. Y. Tsymbal, *Phys. Rev. Lett.* **2005**, *94*, 246802.
[22] R. Meyer, R. Waser, *J. Appl. Phys.* **2006**, *100*, 051611.
[23] A. Q. Jiang, C. Wang, K. J. Jin, X. B. Liu, J. F. Scott, C. S. Hwang, T. A. Tang, H. B. Lu, G. Z. Yang, *Adv. Mater.* **2011**, *23*, 1277.
[24] T. Choi, S. Lee, Y. J. Choi, V. Kiryukhin, S.-W. Cheong, *Science* **2009**, *324*, 63.
[25] C. Wang, K.-J. Jin, Z.-T. Xu, L. Wang, C. Ge, H.-B. Lu, H.-Z. Guo, M. He, G.-Z. Yang, *Appl. Phys. Lett.* **2011**, *98*, 192901.
[26] J. Lee, M. Jo. D.-J. Seong, J. Shin, H. Hwang, *Microelectron. Eng.* **2011**, *88*, 1113.
[27] H. Béa, M. Bibes, A. Barthélémy, K. Bouzehouane E. Jacquet, A. Khodan, J.-P. Contour, S. Fusil, F. Wyczisk, A. Forget, D. Lebeugle, D. Colson, M. Viret, *Appl. Phys. Lett.* **2005**, *87*, 072508.
[28] L. You, N. T. Chua, K. Yao, L. Chen, J. Wang, *Phys. Rev. B* **2009**, *80*, 024105.
[29] J. Wang, J. B. Neaton, H. Zheng, V. Nagarajan, S. B. Ogale, B. Liu, D. Viehland, V. Vaithyanathan, D. G. Schlom, U. V. Waghmare, N. A. Spaldin, K. M. Rabe, M. Wuttig, R. Ramesh, *Science* **2003**, *299*, 1719.
[30] J. W. Park, S. H. Beak, P. Wu, B. Winchester, C. T. Nelson, X. Q. Pan, L. Q. Chen, T. Tybell, C. B. Eom, *Appl. Phys. Lett.* **2010**, *97*, 212904.
[31] M. Ben-Chorin, F. Möller, F. Koch, *J. Appl. Phys.* **1995**, *77*, 4482.
[32] D.-H. Kwon, K. M. Kim, J. H. Jang, J. M. Jeon, M. H. Lee, G. H. Kim, X.-S. Li, G.-S. Park, B. Lee, S. Han, M. Kim, C. S. Hwang, *Nat. Nanotechnol.* **2010**, *5*, 148.
[33] D. S. Jeong, H. Schroeder, R. Waser, *Appl. Phys. Lett.* **2006**, *89*, 082909.
[34] S. J. Clark, J. Robertson, *Appl. Phys. Lett.* **2007**, *90*, 132903.
[35] C. B. Eom, R. B. V. Dover, J. M. Phillips, D. J. Werder, J. H. Marshall, C. H. Chen, R. J. Cava, R. M. Fleming, D. K. Fork, *Appl. Phys. Lett.* **1993**, *63*, 2570.
[36] T. Nakamura, Y. Nakao, A. Kamisawa, H. Takasu, *Appl. Phys. Lett.* **1994**, *65*, 1522.
[37] J. F. M. Cillessen, M. W. J. Prins, R. M. Wolf, *J. Appl. Phys.* **1997**, *81*, 2777.
[38] Z. Zhong, Y. Sugiyama, H. Ishiwara, *Jpn. J. Appl. Phys.* **2008**, *47*, 6448.